Available online at www.sciencedirect.com
SCIENCE DIRECT®
Journal of Nuclear Materials 344 (2005) 246–253
journal of nuclear materials
www.elsevier.com/locate/jnucmat

A Knudsen cell-mass spectrometer facility to investigate oxidation and vaporisation processes in nuclear fuel

J.-P. Hiernaut, J.-Y. Colle, R. Pflieger-Cuvellier, J. Jonnet, J. Somers, C. Ronchi *

European Commission, Joint Research Centre, Institute for Transuranium Elements, P.O. Box 2340, 76125 Karlsruhe, Germany

Abstract

Vaporisation processes in uranium oxide fuel were investigated under controlled oxidation conditions. A Knudsen cell with a mass spectrometer was adapted to feed an adjustable oxygen flux up to temperatures of 1900 K producing an oxygen pressure in the cell ranging up to 1000 Pa. Experiments were carried out on fresh and irradiated fuels, both pre-oxidised to U_3O_8 or oxidised online in the Knudsen cell, to measure effects associated with fuel sublimation in the form of different uranium-bearing oxides. Mass spectrometry, electromotive force measurements and thermo-gravimetric analysis were used to determine the vapour equilibrium conditions at fixed free oxygen potentials.

1. Introduction

The reported work is aimed at investigating the vaporisation processes of actinides and fission products from irradiated nuclear fuel under oxidising conditions, processes that may lead, during hypothetical reactor accidents, to conspicuous radionuclide dispersion in the environment. The project is part of the priority action 'Safety of the Nuclear Fuel Cycle' of the 6th Research Framework Programme of the European Commission, and its final objective is to obtain thermodynamic and kinetic data of irradiated fuel up to very high burnups.

The first round vaporisation measurements reported in this paper show that it is possible to simulate and measure, in a laboratory device consisting of a Knudsen cell equipped with a mass spectrometer, non-congruent vaporisation of irradiated uranium oxide fuel under highly oxidising conditions, by maintaining satisfactory monitoring and control of the sample oxygen potential. Experiments were carried out in a dedicated lead-shielded facility where highly α–γ active samples can be thermally oxidised up to high temperatures.

2. Experiment

The evolution of reactor irradiated uranium dioxide during thermal excursions is to a large extent governed by the oxygen potential, $\Delta G(O_2)$, established in the environment until thermodynamic equilibrium is achieved. In the analysis of accidental fuel oxidation, both equilibrium and reaction kinetics aspects intervene. In the case of highly oxidized states of uranium these aspects are presently poorly known even in non-irradiated UO_{2+x}. Therefore, in a first set of experiments, oxygen potential and vapour pressure of sintered samples of U_3O_8 were measured in a Knudsen cell (KC) as functions of temperature, with the purpose of maintaining as closely as

* Corresponding author. Tel.: +49 7247 951 402; fax: +49 7247 951 99369.
E-mail address: ronchi@itu.fzk.de (C. Ronchi).

0022-3115/$ - see front matter © 2005 Elsevier B.V. All rights reserved.
doi:10.1016/j.jnucmat.2005.04.050

possible chemical equilibrium and pre-fixed oxide compositions under strongly non-congruent sample vaporisation conditions.

2.1. Knudsen cell setup

2.1.1. Mass spectrometer

Fig. 1 shows the sketch of the Knudsen cell (KC) made of alumina (h = 21 mm, ∅ = 11 mm) with different conical orifices of 0.2–1 mm ∅, and 0.1 mm edge thickness (corresponding to a cell Clausing factor between 0.95 and 0.98 at the experiment temperatures).

The specimen temperature was measured with gained thermocouples up to 2300 K, and with a monochromatic pyrometer at higher temperatures. The accuracy of the sample temperature was verified from the thermal arrest plateau on cooling of molten silver, gold and platinum – an additional check being provided by comparison of the slope of the Arrhenius plot of the sublimation rate of silver with its well established vaporisation enthalpy.

A quadrupole mass spectrometer is placed in a chamber immediately above the cell and is evacuated to an ultra-high vacuum by a differential pumping system across the 5 mm ∅ connection with the furnace vessel. Though the geometry of the setup is symmetrical and compact – the mass spectrometer ionisation source being positioned only 50 mm above the effusion-beam orifice – the calculated spatial molecular flow did not provide a satisfactory evaluation of the effective effusion rate from the MS signals; a more precise empirical calibration was obtained with a number of standards. For condensable species, the integrated signals were measured from total vaporisation of known quantities of pure materials. The calibration factor was then extended to other species by using the respective ionisation yields expressed in term of the individual appearance potentials and ionisation cross-sections. Furthermore, in a number of cases it was possible to achieve total vaporisation of the sample, and hence, if its chemical composition and weight were known, the calibration factor could be validated. Agreement of better than 10% was normally found between the two calibration methods.

The calibration for gases, whose behaviour is essentially different from that of condensable species,[1] was made by measuring the integrated MS signals and the gamma activity of a known quantity of ^{85}Kr flowing through the KC and collected in a liquid nitrogen cold trap. The precision of the calibration factor for gas is worse than that of condensable species due to the perturbations brought about by the furnace pressure, the pumping speed and the effusion temperature.

More complex is the determination of the effusion rate of polyatomic molecules that may decompose into fragments in the MS ion source. A more elaborated method was applied to solve this problem. If, for a given molecular species, the fragmentation/ionisation ratio is small, first-order corrections can be applied to reconstruct the original neutral molecule concentration, as, e.g., described in Ref. [1]. If the molecules are to a large extent fragmented (as in the case of UO_3) the measurements must be deployed starting from low ionising electron energies, and investigating the increase in the fragment concentrations as the electron energy is gradually augmented (an example is illustrated in a following paragraph). However, this procedure is hardly practicable if the fragmentation product is a gas, for which the ionisation yield is much higher and less precise than that of condensable fragments. In our specific case, this entails substantial errors in the evaluation of the effective partial pressure of oxygen. For this reason an effort was made to obtain the oxygen pressure in the cell with an independent method described below.

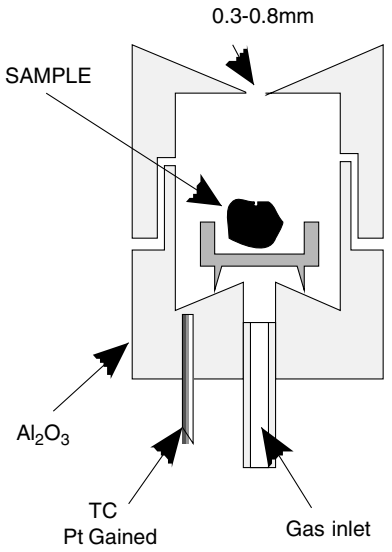

Fig. 1. Schema of the Knudsen cell.

2.1.2. Gas control

The main experimental difficulty is to control fast, highly non-congruent vaporisation of UO_{2+x}. Experiments are planned with two settings: constant sample composition and constant oxygen partial pressure. In both cases a precise and prompt feedback on the gas inlet system is required. The schema of the gas inlet system is shown in Fig. 2. The resulting pressure in the KC is evaluated as follows:

[1] A non-condensable gas atom or molecule has a much higher ionization probability than a condensable one since it survives outside its original molecular beam in a thermalised state and may pass again and again through the ion source until it is evacuated by the pump.

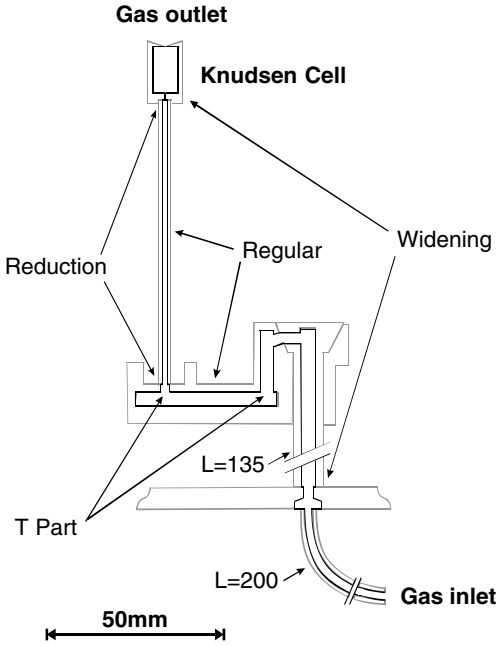

Fig. 2. Schema of the gas-inlet pipeline.

A laminar flow Q is produced in the pipe with an inlet pressure p_1 and a conductance C building along the pipe a charge loss $(p_1 - p_2) = Q/C$. The integral value of C for a circuit of varying section, temperature and singularities was calculated from the design data of the constituting ith segments [2] whose contribution is expressed by a law of type:

$$C_i = \frac{\pi^4 \bar{p}_i D_i^4}{128 \eta_i L_i}, \tag{1}$$

where L_i and D_i are, respectively, length and diameter of the pipe segment; $\eta_i = \eta(T_i)$ is the local viscosity of the gas. Under the examined experimental conditions, the Reynolds number is to be everywhere <4000 in order that laminar flow conditions are realised. However, in the Knudsen cell the flow changes from laminar to molecular, and this entails some shortcuts in coupling the fluid dynamic equation [3]. However, if the product Dp is >50 cm Pa, the precision of Eq. (1) is better than 10%. Fig. 3 shows the resulting relationship between a pre-fixed pressure at the pipe entrance and that in the KC, together with the resulting inflow rate. By experimental verification of these curves it was realised that a control of the oxygen pressure in the KC was possible, but mainly limited by the effective vaporisation rate.

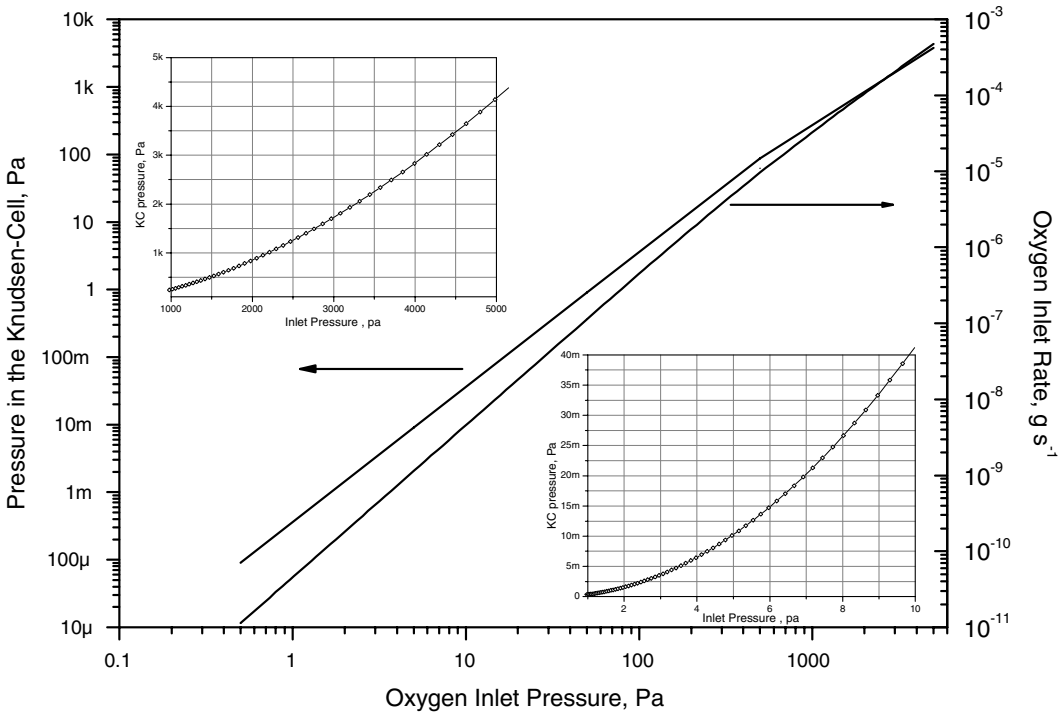

Fig. 3. Oxygen pressure in the Knudsen cell as a function of the pipe entrance pressure. The resulting gas flow rate is also plotted. Orifice diameter: 0.5 mm, temperature at the pipe hot end: 1500 K. The insets show two segments of the pressure curve with a linear scale.

2.2. Determination of the sample stoichiometry and reference samples

The stoichiometry of the samples was deduced from the oxygen potential [4] obtained from the electrochemical potential, E, measured in an electromotive force (EMF) micro cell (sketched in Fig. 4). The sample is nominally tightly closed in the very small cell volume, where vapour equilibrium conditions must be established. Since, however, the cell is placed in a vacuum, at high temperatures significant oxygen losses may occur, entailing stoichiometry changes in the sample, as shown in the next section. The EMF potential is expressed as:

$$E = \frac{RT}{4F} \ln \frac{\mu_{O_2}^{\text{sample}}}{\mu_{O_2}^{\text{reference}}}. \quad (2)$$

The oxygen activity in the sample was measured from the reference REDOX couple Fe/FeO given in Ref. [5]:

$$\Delta G^{O}_{FeO} = -529\,778 + 130.584T \quad (3)$$

and

$$\Delta G^{O}_{UO_{2+x}} = 4FE + 529\,778 - 130.583T, \quad (4)$$

where T is the temperature in K, F is the Faraday constant (96484.6 C/mole) and E is the EMF of the cell in Volt.

Reference measurements of the equilibrium vapour pressure of non-congruently vaporising oxides were carried out on U_3O_8 samples prepared by sintering green pellets at 1450 K in a 0.1 MPa oxygen atmosphere during 6 h. XRD analysis shows that after this treatment, in conjunction with the initial orthorhombic phase U_3O_8 (space group C222) measured in the green pellet, a second minor orthorhombic phase interpretable as a lattice of space group Cmcm was observed. This phase has definitely a lower lattice density, and is likely formed by an oxide of type U_3O_{8+x} hosting interstitial oxygen, a conjecture supported by the EMF results reported below.

In subsequent experiments, samples of fresh and reactor irradiated UO_2 were treated at 860 K under up to 100 Pa oxygen pressure in the KC. The samples, in the form of coarsely crushed sintered pellets, had a weight of the order of 100 mg, whilst those of irradiated fuel consisted of a few fragments of 10–20 mg total weight. The vapour pressure and the sample composition were measured at various temperatures under a constant oxygen flux in the cell. Comparative tests show that cell volume and aperture sizes were suitable for a Knudsen-effusion regime to be attained even with such small samples.

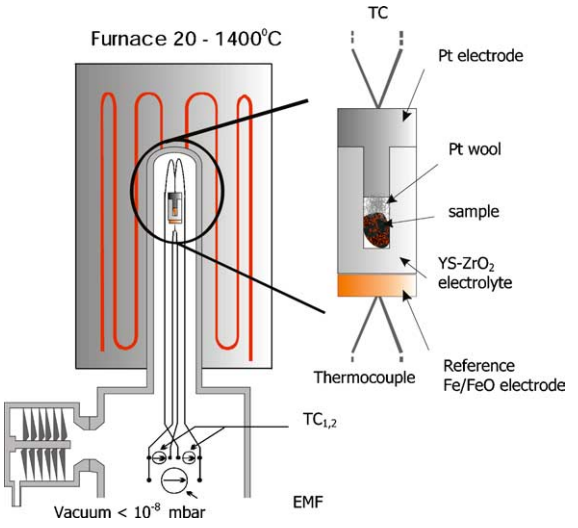

Fig. 4. Sketch of the EMF measurement system: the sample in the galvanic cell is heated under vacuum up to a predefined temperature measured by two thermocouples at the two extremities of the cell. The electromotive force is created in the solid electrolyte (ZrO_2–Y_2O_3) by the oxygen potential difference between the sample and the reference REDOX couple.

3. Knudsen cell measurements: Vapour composition

The graph in Fig. 5 shows an example of vapour analysis obtained from the mass spectrometer measurements during an experiment where a UO_2 sample, after oxidation at 860 K in an oxygen pressure of 20 Pa, was submitted to two step-like temperature increases, respectively to 1500 K and 1650 K, by maintaining a constant oxygen inflow. After oxidation, the MS signals show that vapours can be detected already at temperatures

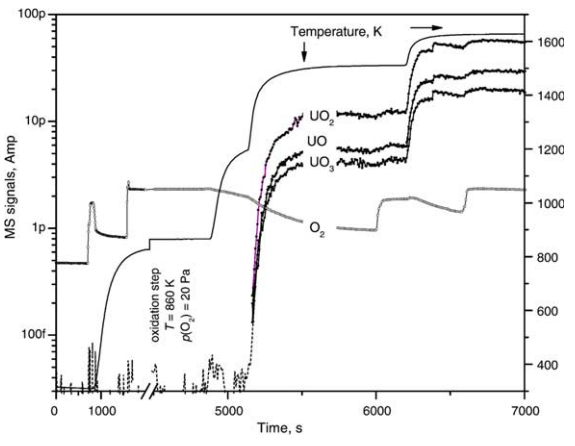

Fig. 5. Mass spectrometric measurements of the evolution of the O_2^+, UO^+, UO_2^+ and UO_3^+ ion signals under controlled oxidation conditions for an ionising electron energy of 40 eV. Note that despite being UO_3(g) the major vapour species, the UO_3^+ ion current is the lowest and is largely exceeded by that of the ionisation fragments UO_2^+ and UO^+.

(≈1000 K) at which in the stoichiometric oxide the vapour pressures are by far under the MS detection limit.

One can see that, as temperature is increased, the sublimation rate and the reactivity of U_3O_8 increase, and the oxygen pressure established by a constant O_2 inflow drops down, indicating that the this becomes insufficient to compensate for the oxygen losses due to non-congruent vapour effusion. A prompt gas inlet regulation was then used to maintain pre-fixed oxygen pressure in the cell, as shown in the graph. However, at temperatures above 1600 K the effective reduction/oxidation reaction times of U_3O_8 are shorter than a few tens of seconds for typical coarsely granulated samples. This entails experimental difficulties, especially if time consuming vapour composition measurements are to be carried out in conjunction with flow adjustments.

Furthermore, though UO_3(g) is largely predominant in the vapour, the highest measured MS signal is that of UO_2^+(g), a species that is in reality a fragmentation product of UO_3(g). The same origin have the UO^+(g) and the (much lower) U^+(g) signals – the latter not plotted in this figure. Thus, due to the high rate of dissociation of UO_3(g), the fraction of uranium-bearing ions largely differs from the real composition of the vapour.

Fig. 6 illustrates the typical MS measurement conditions encountered in vapour composition measurements of U_3O_{8-x} in the presence of highly non-congruent vaporisation under constant flux conditions. To obtain the real vapour composition the ionising electron energies have been gradually increased. Between 0 and 10 eV only the UO_2(g) molecules are ionised (first ionisation potential E_1 = 5.4 eV) and detected. Above the first ionisation potential of UO_3(g) (10.8 eV) the trioxide ions

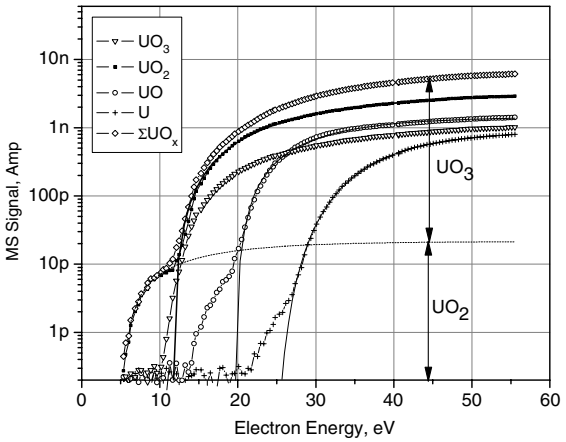

Fig. 6. Appearance potentials of the different uranium-bearing ion species created by ionisation of the vapour above U_3O_8 at 1848 K as a function of the applied electron energy.

Table 1
Apparent ionisation and dissociation energies of uranium oxide ions, as measured in the ion source of the mass spectrometer

Reactions	Measured (eV)	Literature (eV)
$UO_2 + e^- \rightarrow UO_2^+ + 2e^-$	5.3	5.4
$UO_2 + e^- \rightarrow UO^+ + O + 2e^-$	13.5	13.4
$UO_2 + e^- \rightarrow U^+ + O_2 + 2e^-$	21.3	21.7
$UO_3 + e^- \rightarrow UO_3^+ + 2e^-$	10.3	10.8
$UO_3 + e^- \rightarrow UO_2^+ + O + 2e^-$	11.6	11.3
$UO_3 + e^- \rightarrow UO^+ + O_2 + 2e^-$	19.6	19.3
$UO_3 + e^- \rightarrow U^+ + O_2 + O + 2e^-$	25.7	27.6

appear, but at effectively the same energy the UO_2^+(g) vs. energy signal shows a clear slope discontinuity, indicating a concomitant UO_3(g) dissociation. UO^+(g) and U^+(g) ions appear as additional products of UO_3(g) fragmentation or of secondary fragmentation of UO_2^+(g), as one can see from the curves plotted in the graph. The appearance and dissociation energies of the various uranium oxide ions evaluated from their appearance curves are reported in Table 1 and compared with reference values [6].

Fig. 7 shows the evolution of the vapour composition over U_3O_8 during an experiment were the oxygen partial pressure was maintained constant as far as it was permitted by the MS working conditions. The values of the partial pressure $p(UO_3)$ and $p(O_2)$ are plotted as functions of temperature for the reference compositions U_3O_8, U_4O_9 and UO_2. Three UO_2 samples (one of them irradiated at 50 MWd/t burnup) were then investigated. The effusion of the first one was measured under high vacuum after oxidation to U_3O_8 in the KC at low temperature, whilst the stoichiometric samples were measured during a thermal annealing programme under a controlled oxygen pressure of 20 Pa. The partial vapour pressures over the three samples are close to the U_3O_8 reference curves until approximately 1400 K. Above ≈1500 K the measured partial pressure of oxygen decreases rapidly and, simultaneously, the partial pressure of UO_3(g) decreases crossing at 1500 K the UO_3(g)/U_4O_9(cr) equilibrium curve.[2] At higher temperatures the UO_3(g) pressure asymptoptically decreases towards that of UO_3(g)/UO_2(cr).

The samples initially in the dioxide form, and heated under 20 Pa oxygen, a few minutes after reaching 1200 K display a UO_3(g) pressure effectively equal to that over U_3O_8, though with large random fluctuations. One can see that whilst the fixed pressure of O_2 lies above the $p(O_2)/U_3O_8$(cr) equilibrium, the measured $p(UO_3)$ is close to the $p(UO_3)/U_3O_8$(cr) curve. However,

[2] With the symbol A/B we indicate equilibrium of the gas phase A over the solid B.

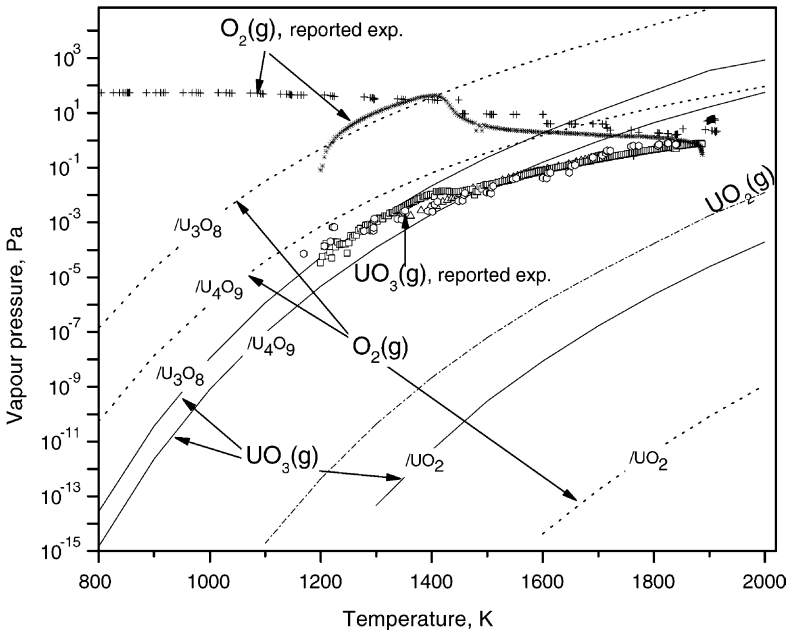

Fig. 7. MS-measured equilibrium vapour pressure of O_2 and UO_3(g) as a function of temperature. The oxygen inlet valve was gradually opened to equilibrate the oxygen partial pressure over U_3O_8. Above approximately 1400 K the maximum allowed flux was insufficient to maintain equilibrium.

when, at higher temperatures, $p(O_2)$ decreases due to non-congruent vaporisation and insufficient oxygen supply, also $p(UO_3)$ decreases, reaching, and finally passing below the $p(UO_3)/U_4O_9$(cr) equilibrium curve, and effectively following the same trend as that of the U_3O_8 sample. This indicates that the oxygen supply was negligible compared to the net losses due to sublimation. This obviously imposes drastic upper limits to the measurement temperatures.

4. Thermal stability of U_3O_8

To measure the equilibrium vaporisation of U_3O_8 at higher temperatures, the Knudsen cell orifice was reduced from 0.5 to 0.3 mm diameter. This enabled measurements to be carried out up to approximately 1900 K. The oxygen leak valve was electronically regulated by the measured oxygen pressure in the KC. The temperature was varied stepwise with sufficiently long plateaux to guarantee chemical equilibrium conditions. Appearance potential curves for the detected ions were taken at every temperature plateau to determine the real vapour composition.

The evolution of $\Delta G(O_2)$ over U_3O_8 samples was measured in parallel with EMF analysis, in the temperature range 300–1300 K. Typical EMF measurement cycles are shown in Figs. 8 and 9. The oxygen potential curve of U_3O_8 obtained after oxidation in air is initially

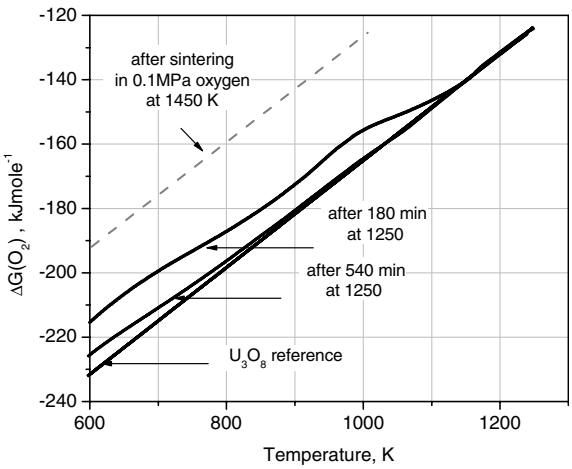

Fig. 8. ΔG_{O_2} of U_3O_{8+x} vs. T measured in the EMF cell during subsequent cycles. After the sixth measurement cycle the sample is reduced to U_3O_{8-x}. Measurements at $T < 560$ K are limited by the too low conductivity of the solid electrolyte.

higher than that of the reference octoxide. However, after a few measurement cycles in the EMF cell, the values obtained are very close to the U_3O_8 reference curve (Fig. 9). Further permanence in the cell at high temperature reduces the sample to U_4O_9. The reduction kinetics at different temperatures is shown in the graph of Fig. 9. With reference to the above mentioned XRD results,

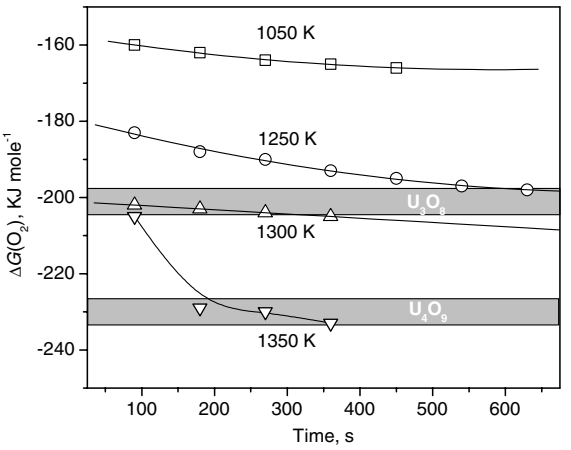

Fig. 9. Kinetics of the sample reduction in the EMF cell at different temperatures.

we can infer that a phase transition occurs between 1000 and 1150 K, corresponding to the reaction:

$$U_3O_{8+x} \rightarrow U_3O_8 + (1/2)xO_2. \quad (5)$$

This phase change is realised by a decrease of $\Delta G(O_2)$ of more than 10 kJ mole^{-1}. The transition temperature is independent of the heating rate and cycle number, if the end temperature remains lower than 1200 K, under this condition the phase transition is perfectly reproducible.

5. Vaporisation of U_3O_8 under constant oxygen pressure

Vapour pressure measurements of U_3O_8 sintered samples at increasing temperatures from 1400 to 1960 K were performed at a constant O_2 pressure of 2000 Pa.

During the first half of each temperature plateau (of ~20 min duration) the different ions corresponding to the gaseous species, O, O_2, U, UO, UO_2, UO_3 were measured in the MS. During the second half, the real composition of the vapour was determined (at a given temperature and for a given oxygen pressure in the cell) from the complete appearance potential curves of UO_3^+(g) in UO_2^+(g), UO^+(g) and U^+(g), as described above.

Fig. 10 shows the vapour composition at a relatively high temperature (1960 K) above UO_{2+x} for different values of x as a function of the oxygen pressure in the cell. Again, the measured points are plotted together with the recommended values for reference oxide compounds. It can be seen that the slope of the logarithmic curve of $p(UO_3)/p(UO_2)$ vs. $p(O_2)$ changes from 1 to 0.5 as the oxygen pressure increases and the ruling reaction gradually changes from $UO_3 \rightarrow UO_2 + O$ to $UO_3 \rightarrow UO_2 + (1/2)O_2$. Fig. 11 shows the total pressure variation of the uranium bearing vapour species with the oxygen pressure in the Knudsen cell. The linear fit of the experimental data of U_3O_8, U_4O_9 and UO_2, at 1960 K, is given by the expression:

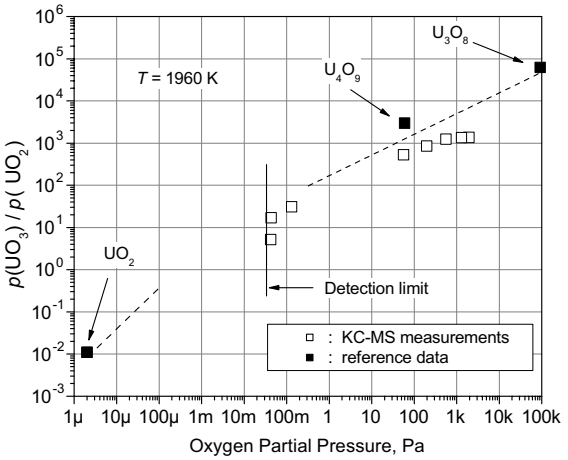

Fig. 10. Vapour composition ($p(UO_3)/p(UO_2)$ above U_3O_8 as a function of $p(O_2)$ in the Knudsen cell at 1960 K. The open symbols represent single experimental measurements, the full symbols the reference averaged values for U_3O_8, U_4O_9 and UO_2. The vertical line shows the detection limit at 1960 K, for a KC orifice of 0.3 mm size.

$$\ln(p_{U_{tot}}) = (1.83 \pm 0.09) + (0.378 \pm 0.015)\ln(p(O_2)). \quad (6)$$

Here the experimental limits are well visible: to maintain stoichiometric U_3O_8 just above 2000 K, one should be

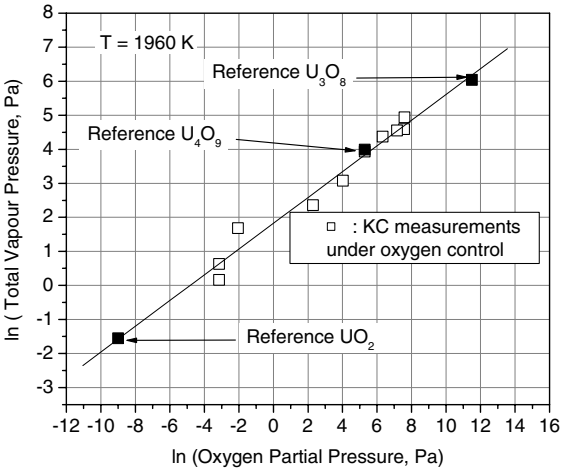

Fig. 11. Total uranium oxides vapour pressure as a function of $p(O_2)$ in the Knudsen cell at 1960 K. The open symbols correspond to single experimental measurements, the full ones are averaged reference values.

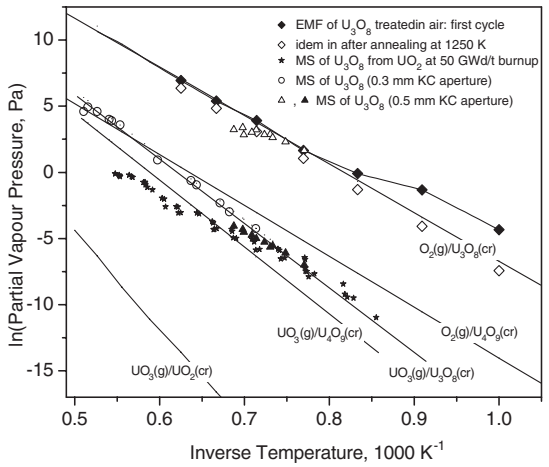

Fig. 12. Arrhenius plot of the measured equilibrium partial pressures, showing the effect of insufficient compensation of the oxygen sublimation losses. U_3O_8 equilibrium could be maintained up to approximately 2000 K is a small KC aperture was used and the sample was sufficiently large. U_3O_8 samples of 10–20 mg weight obtained from high burnup UO_2 could be kept in equilibrium up to approximately 1400 K.

able to increase the oxygen pressure up to several 10^3 Pa in the cell.

Fig. 12 shows a synoptic plot of the partial pressure measurements carried out on fresh and irradiated fuels, in conjunction with EMF measurements of their oxygen potential. Precise measurements of the vapour partial pressures over stoichiometric U_3O_8 indicate that equilibrium could be maintained up to approximately 1400 K. Any effort to increase the oxygen flux does not produce any relevant extension of the viable temperature range, unless the KC aperture size is decreased down to 0.3 mm, whereby, however, deviations from the molecular flow regime will occur at these high pressures. The data points seem, however, to stretch out on the expected curve up to almost 2000 K.

6. Conclusions

A gamma-shielded Knudsen cell with mass spectrometer was designed and constructed to measure the vaporisation rate and the equilibrium vapour pressure of UO_{2+x} nuclear fuel under controlled oxygen partial pressures.

Online oxidation experiments were conducted on as-fabricated and reactor-irradiated uranium oxides up to the highest oxidation states, showing that thermodynamic conditions could be controlled in limited temperature ranges where the equilibrium vapour pressure of the various components could be measured with a good accuracy.

References

[1] F. Capone, J.Y. Colle, J.P. Hiernaut, C. Ronchi, J. Phys. Chem. A 103 (50) (1999) 10899.
[2] R.C. King (Ed.), Piping Handbook, McGraw-Hill, New York, 1973.
[3] W.J. Moore, Physical Chemistry, Prentice Hall, New York, 1955.
[4] T.L. Markin, R.J. Bones, UKAEA Report AERE-R4042 HL 62/2187 (C3), UK, 1962.
[5] D. Labroche, O. Dugne, C. Chatillon, J. Nucl. Mater. 312 (2003) 21.
[6] L.V. Gurvich, V.S. Iorish, D.V. Chekhovsioi, V.S. Yungman, NIST Special Database 5, 'IVTANTHERMO'. CRC, Boca Raton, FL, 1993.